Journal of Sol-Gel Science and Technology 31, 249–252, 2004

Nanostructured Ion-Selective MCM-48 Membranes

RIAAN SCHMUHL, SANKHANILAY ROY CHOWDHURY, JOHAN E. TEN ELSHOF*,
ALBERT VAN DEN BERG AND DAVE H.A. BLANK
University of Twente, MESA$^+$ Research Institute & Faculty of Science and Technology, P.O. Box 217, 7500 AE Enschede, the Netherlands

Abstract. Templated MCM-48 silica was prepared using CTAB as surfactant. The MCM-48 powders and thin films were characterized by different techniques. MCM-48 layers were deposited on macroporous α-alumina supports and silicon nitride microsieves. The water permeability of MCM-48 was compared with the permeability of conventional mesoporous γ-alumina membranes. The applicability of MCM-48 as ion-selective electric field-driven switchable interconnect for microfluidic devices was demonstrated.

Keywords: membrane, silica, MCM-48, permeability, permselectivity

Introduction

Mesoporous inorganic membranes exhibit a number of desirable physical properties such as high mechanical strength, chemical and thermal stability. However, conventional sol-gel derived mesoporous membranes such as γ-alumina have a disordered pore structure with a relatively wide pore size distribution and a high tortuosity [1, 2], which affects the intrinsic separation selectivity and permeability of the separating layer negatively. The mesopore architecture can be improved significantly by employing template-directed synthesis methods [3]. Mesoscopically ordered micellar templates can yield a high porosity and a narrow pore size distribution in the final mesoporous layer. Well-known examples of these are MCM-type materials [4]. A disadvantage of the 2D hexagonal MCM-41 structure for membrane applications is that the surfactant assemblies tend to align themselves parallel to the membrane interfaces during drying, which finally results in ordered pore structures with main transport paths parallel to the substrate [5]. On the other hand the MCM-48 structure is a potential candidate for membrane applications. Theoretical calculations indicate that it has a 3D interconnected pore geometry [6], so that MCM-48 is expected to have a low tortuosity in the direction perpendicular to the membrane surface.

The applicability of silica MCM-48 thin layers for liquid phase ion separation processes is demonstrated in the present paper. The small pore size and narrow pore size distribution allow complete double layer overlap inside the membrane pores at relatively high ionic strengths. This makes MCM-48 a suitable material for application as electric field-driven ion-selective switchable interconnect for microfluidic devices [7], or as salt retention membrane in desalination processes [8].

Experimental

Surfactant-templated silica sols were synthesized using the cationic surfactant cetyl-trimethyl-ammonium bromide (CTAB, Aldrich) and tetra-ethoxy-orthosilicate (TEOS, Aldrich) derived sols as described elsewhere [9]. Spin coating and dip coating were used to deposit thin silica films on dense silicon wafers, α-alumina supports, and silicon nitride microsieves. The layers were dried at room temperature and subsequently calcined at 450°C in air for 2 h. γ-Alumina was prepare as described elsewhere [1, 8]. Macroporous α-Al_2O_3 supports (2 mm thick, Ø 39 mm, pore size 100 nm,

*To whom all correspondence should be addressed.

porosity 30%) were made via colloidal filtration of α-Al_2O_3 particles [8]. Silicon nitride Microsieves® (0.5×0.5 cm, porosity 30%, 1 μm thick, with circular perforations Ø 0.5 or 1.2 μm) were supplied by Aquamarijn Micro Filtration (The Netherlands).

X-ray diffraction (XRD) patterns of thin silica films were recorded using a Philips SR5056 with Cu Kα radiation. Nitrogen sorption measurements (Micromiretics) were performed at 77 K on dried and calcined silica powders. SEM was performed with a LEO 1550 FEG SEM. Permporometry experiments with cyclohexane were performed in a homemade set-up [10]. Water fluxes were measured in a dead end nanofiltration cell [8]. Electric field mediated ion transport experiments with fluorescein (Fl^{2-}, Fluka), methylviologen (MV^{2+}, Aldrich) and *d*-tryptophan (Aldrich) were carried out in a set-up described elsewhere [11]. A dc potential difference ΔV, defined as the potential at the receive (permeate) side relative to the potential at the feed side, was imposed over the membrane using external Pt electrodes separated by 4 mm. The pH was maintained at 7.8–8.2 with a NaH_2PO_4/Na_2HPO_4 buffer solution. Prior to all experiments the membranes were left in water or buffer solution to ensure complete wetting.

Results and Discussion

Figure 1 shows the XRD pattern of 100 nm thick uncalcined and calcined silica films after deposition on a dense silicon wafer. The low-angle reflection at 2θ 2.4–3.2° and a series of overlapping weak reflections at 2θ 4.5–6° matched the pattern of mesoporous MCM-48 [11] with a unit cell $a \sim 9.2$ nm. The marked sharp peaks were probably from crystalline CTAB and they disappeared upon calcination. The sample retained its mesostructure after calcination but with smaller *d*-spacing ($a \sim 6.3$ nm). No diffraction peaks were observed in 20–70 nm films that were deposited on α-alumina supports, which is probably due to the roughness and texture of the support, which promotes local nucleation and growth of ordered domains with different orientations at length scales that are too small to be detectable by XRD. Permporometry on alumina-supported MCM-48 membranes indicated that the calcined silica films were porous, defect-free and had a Kelvin radius <1.7 nm. This is in agreement with nitrogen sorption data on unsupported MCM-48 powders, from which an average pore diameter of 2.3–2.6 nm was calculated.

The water flux through a 65–70 nm thick α-alumina supported MCM-48 membrane is shown in Fig. 2. The permeability of water through supported MCM-48 was higher than that through a conventional supported γ-alumina membrane. The linear relationship between the volumetric flux j_v and applied pressure Δp is in agreement with Darcy's law

$$j_v = -\frac{k_m}{\eta}\Delta p, \tag{1}$$

where η is the liquid viscosity and k_m the permeability. For a stacked membrane the overall permeability is related to the permeabilities of the support k_α and top layer k_β via

$$k_m^{-1} = k_\alpha^{-1} + k_\beta^{-1}. \tag{2}$$

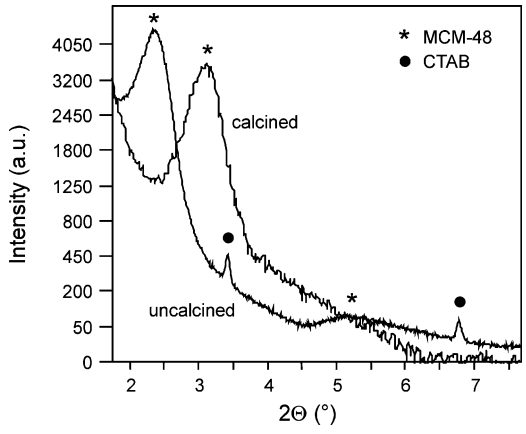

Figure 1. XRD diagrams of uncalcined air-dried and 450°C calcined silica layer on dense silicon wafer.

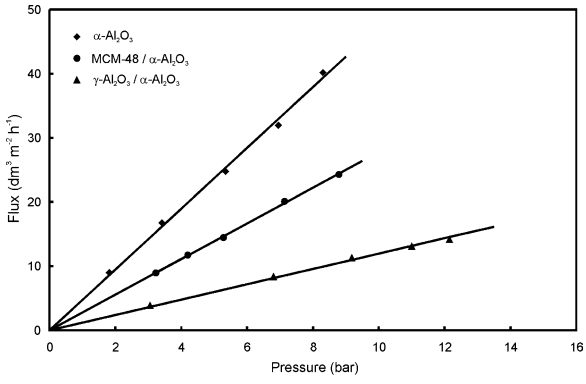

Figure 2. Water fluxes through α-Al_2O_3 supported silica MCM-48, α-Al_2O_3-supported γ-Al_2O_3, and α-Al_2O_3 support.

From the data shown in Fig. 2 it can be calculated that the permeability of the α-Al_2O_3 support is $k_\alpha = (1.17 \pm 0.03) \cdot 10^{-14}$ m. The permeabilities k_β of the MCM-48 and γ-Al_2O_3 layers are $(1.66 \pm 0.06) \cdot 10^{-14}$ m and $(3.96 \pm 0.20) \cdot 10^{-15}$ m, respectively. Since the γ-alumina layer is ~ 1 μm thick, has a porosity of 55% and a tortuosity of 5–15 [2], while the MCM-48 has a total porosity of $\sim$60% and a lower tortuosity, it appears that the much higher permeability of the MCM-48 layer should be attributed mainly to its much smaller layer thickness.

When the differences in mesoporous layer thickness L_β are taken into account by comparing $k_\beta L_\beta$ instead of k_β, the intrinsic permeability of the MCM-48 structure is $\sim$5 times lower than that of γ-alumina. Possibly this relatively low value of $k_\beta L_\beta$ in MCM-48 is caused by a lack of direct mesopore connectivity, which was also observed in 3D hexagonal silica [13]. In that case liquid transport will take place at least partly by diffusion through highly resistive micropores in the mesopore walls that act as interconnects for the more permeable mesopores. In contrast to MCM-48, γ-alumina does not have microporosity.

Figure 3 shows SEM pictures of calcined MCM-48 layers that were deposited on Microsieves by spin coating. The MCM-48 layers can be seen to penetrate the perforations of the sieves and are about 650 nm thick in the center of the perforations. Figure 4 shows the ionic fluxes of fluorescein (Fl^{2-}, ion charge -2) and methylviologen (MV^{2+}, ion charge $+2$) through these membranes versus the applied potential difference between the Pt electrodes ΔV. The inset of Fig. 4 shows how the concentration of fluorescein (Fl^{2-}) at the receive side increased almost linearly with time after a positive ΔV had been imposed. On the other hand no noticeable concentration increase occurred in 8 h time when $\Delta V \leq 0$. The opposite trend was observed for MV^{2+}. In all cases measurable ionic fluxes were directed towards an oppositely charged electrode at the receive side of the membrane, which strongly suggests that transport occurs mainly by an ion migration mechanism [14]. The absence of a noticeable flux for both ionic species under field off conditions ($\Delta V = 0$) indicates that transport by Fick diffusion is limited. Similar transport experiments with uncharged *d*-tryptophan did not show significant fluxes within experimental error under either field-on or field-off conditions, which suggests that solvent and ion transport by electroosmotic flow is negligible.

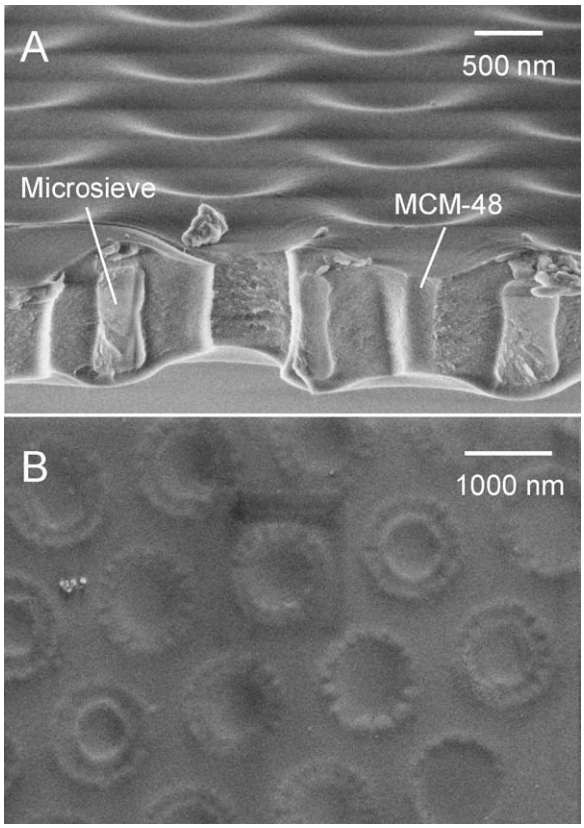

Figure 3. (A) Microsieve (1.2 μm perforations) with MCM-48 layer; (B) top view of MCM-48 layer on Microsieve with 500 nm perforations.

It is noted that the MV^{2+} flux at $\Delta V = -2$ V was much higher than the observed Fl^{2-} flux at $\Delta V = +2$ V. Upon defining the ionic permeability P_i of the membrane towards an ion i by

$$j_i = P_i \frac{\Delta c_i}{L}, \tag{3}$$

where j_i is the ionic flux, Δc_i the ion concentration difference over the membrane, and L the average membrane thickness ($L = 970$ nm), it follows that $P_{Fl(2-)} = (3.7 \pm 0.3) \cdot 10^{-8}$ cm^2/s at $\Delta V = +2$ V and $P_{MV(2+)} = (1.1 \pm 0.1) \cdot 10^{-6}$ cm^2/s at $\Delta V = -2$ V. The roughly 30 times higher permeability of MV^{2+} can be explained by the combination of membrane surface charge and the occurrence of double layer overlap in the membrane pores. The double layer thickness can be estimated from the Debye length κ^{-1} [14]. For the experiments described here, κ^{-1} is approximately 3–4 nm. Since the membrane pore size

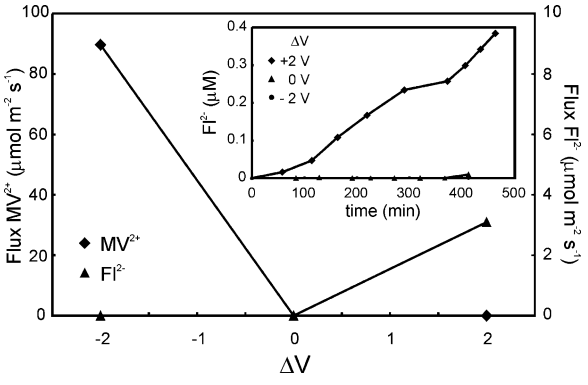

Figure 4. Fluxes of fluorescein (Fl^{2-}) and viologen (MV^{2+}) versus electrode potential difference ΔV. Feed side probe concentration 0.8 mM. The inset shows the concentration increase of Fl^{2-} at the receive side versus time at $\Delta V = -2$, 0 and $+2$ V.

is 2.3–2.6 nm, the double layer spans the width of the pores entirely. And as the pore surface of silica at pH 8 is negatively charged [15], the diffuse double layer will consist mainly of positively charged ions. Hence, a higher ionic permeability is expected for cations.

Conclusions

Defect-free MCM-48 layers were deposited on macroporous α-alumina supports and silicon nitride microsieves. The water permeability of the MCM-48 layer was higher than that of a conventional γ-alumina layer due to its smaller layer thickness. The application of MCM-48 membranes as ion-selective gates for microfluidic applications was demonstrated. The transport of cations and anions could be switched on and off with a variable electric field. The predominant cation permselectivity of MCM-48 was attributed to a combination of negative surface charge on the silica pore walls and the occurrence of double layer overlap inside the pores.

Acknowledgment

Aquamarijn is gratefully acknowledged for providing Microsieves.

References

1. A.F.M. Leenaars, K. Keizer, and A.J. Burggraaf, J. Mater. Sci. **19**, 1077 (1984).
2. A.F.M. Leenaars and A.J. Burggraaf, J. Membrane Sci. **24**, 245 (1985).
3. Q. Huo, D.I. Margolese, and G.D. Stucky, Chem. Mater. **8**, 1147 (1994).
4. C.T. Kresge, M.E. Leonowicz, W.J. Roth, J.C. Vartuli, and J.S. Beck, Nature **359**, 710 (1992).
5. M. Klotz, A. Ayral, C. Guizard, and L. Cot, Sep. Purif. Technol. **25**, 71 (2001).
6. M.W. Anderson, Zeolites **19**, 220 (1997).
7. T.-C. Kuo, D.M. Cannon, Y. Chen, J.J. Tulock, M.A. Shannon, J.V. Sweedler, and P.W. Bohn, Anal. Chem. **75**, 1861 (2003).
8. S. Roy Chowdhury, J.E. ten Elshof, N.E. Benes, and K. Keizer, Desalination **144**, 41 (2002).
9. I. Honma, H.S. Zhou, D. Kundu, and A. Endo, Adv. Mater. **12**, 1529 (2000).
10. G.Z. Cao, J. Meijerink, H.W. Brinkman, and A.J. Burggraaf, J. Membrane Sci. **83**, 221 (1993).
11. S. Roy Chowdhury, R. Schmuhl, K. Keizer, A. van den Berg, J.E. ten Elshof, and D.H.A. Blank, in *Self-Assembled Nanostructured Materials*, edited by C.J. Brinker, M. Antonietti, Y. Lu, and C. Bai (Materials Research Society, Pittsburg, 2003).
12. J. Xu, Z. Luan, H. He, W. Zhou, and L. Kevan, Chem. Mater. **10**, 3690 (1998).
13. M. Klotz, S. Besson, C. Ricolleau, F. Bosc, and A. Ayral, in *Membranes—Synthesis, Properties and Applications*, edited by V.N. Burganos, R.D. Noble, M. Asaeda, A. Ayral, and J.D. LeRoux (Materials Research Society, Pittsburg, USA, 2003), p. 123.
14. P.J. Kemery, J.K. Steehler, and P.W. Bohn, Langmuir **14**, 2884 (1998).
15. A.J. Pierre, *Introduction to Sol-Gel Processing* (Kluwer, Dordrecht, 1998), p. 62.